AGU PUBLICATIONS

JGR

Journal of Geophysical Research: Space Physics

RESEARCH ARTICLE

10.1002/2014JA020476

Special Section:
Origins and Properties of Kappa Distributions

Terrestrial lion roars and non-Maxwellian distribution

M. N. S. Qureshi[1], Warda Nasir[1,2], W. Masood[3,4], P. H. Yoon[5,6], H. A. Shah[2], and S. J. Schwartz[7]

[1]Department of Physics, GC University, Lahore, Pakistan, [2]Department of Physics, Forman Christian College, Lahore, Pakistan, [3]COMSATS Information of Technology, Islamabad, Pakistan, [4]National Center for Physics, Islamabad, Pakistan, [5]Institute for Physical Science and Technology, University of Maryland, College Park, Maryland, USA, [6]School of Space Research, Kyung Hee University, Seoul, South Korea, [7]Blackett Laboratory, Imperial College London, London, UK

Abstract Lion roars are low-frequency (~100 Hz) whistler waves frequently observed in the Earth's magnetosheath. By analyzing both wave and electron data from the Cluster spacecraft, and comparing with linear Vlasov kinetic theory, Masood et al. (2006) investigated the underlying cause of the lion roar generation. However, the analysis based upon the bi-Maxwellian distribution function did not adequately explain the observations qualitatively as well as quantitatively. This outstanding problem is revisited in the present paper, and a resolution is put forth in which, the flat-top non-Maxwellian distribution function with a velocity power law energetic tail, known as the (r, q) distribution, or the generalized kappa distribution is employed. Upon carrying out the linear stability analysis of the (r, q) distribution against the whistler wave perturbation, and upon comparison with the Cluster data, good qualitative and quantitative agreements are found between theory and data.

Key Points:
- Lion roar emission is explained by (r, q) distribution
- Bi-Maxwellian model cannot always explain observation
- The (r, q) model satisfactorily resolves observational uncertainties

Correspondence to:
P. H. Yoon,
yoonp@umd.edu

Citation:
Qureshi, M. N. S., W. Nasir, W. Masood, P. H. Yoon, H. A. Shah, and S. J. Schwartz (2014), Terrestrial lion roars and non-Maxwellian distribution, *J. Geophys. Res. Space Physics*, *119*, 10,059–10,067, doi:10.1002/2014JA020476.

Received 4 AUG 2014
Accepted 1 DEC 2014
Accepted article online 3 DEC 2014
Published online 27 DEC 2014

1. Introduction

The study of waves found in the Earth's magnetosheath is important, since these waves may lead to the redistribution of energy and momentum in the plasma. Furthermore, the magnetosheath waves eventually determine what kind of shocked solar wind plasma is transported to the magnetosphere. Satellite observations indicate the ubiquitous presence of narrowband electron whistler waves termed the "lion roars" [*Smith*, 1969; *Smith and Tsurutani*, 1976; *Thorne and Tsurutani*, 1981; *Anderson et al.*, 1982; *Tsurutani et al.*, 1982; *Moreira*, 1983; *Rodriguez*, 1985; *Lee et al.*, 1987; *Zhang et al.*, 1998; *Baumjohann et al.*, 1999; *Maksimovic et al.*, 2001; *Masood et al.*, 2006].

Thorne and Tsurutani [1981] conjectured for the first time that whistler waves with electron temperature anisotropy could be the progenitors of lion roars observed in the magnetosheath. The study was conducted in the era when observations were made by dint of a single spacecraft, and therefore, it was not possible to remove the spatiotemporal ambiguity in the data. Following *Thorne and Tsurutani* [1981], various theoretical aspects associated with the lion roar generation have been reported in a number of papers [e.g., *Moreira*, 1983; *Lee et al.*, 1987; *Baumjohann et al.*, 1999].

In a relatively recent paper, *Masood et al.* [2006] revisited the problem by making a comparison of the kinetic theory of bi-Maxwellian electrons with the multispacecraft data of Cluster that was capable of resolving the spatiotemporal ambiguity. The authors also used the electron velocity distribution obtained from Cluster Plasma Electron and Current Experiment (PEACE) data [*Johnstone et al.*, 1997] in order to obtain a deeper understanding of the generation of lion roars. However, it was found that except for some instances, the agreement between the theory and data was not seen. The major cause of the discrepancy was the presence of lion roars for long intervals in the data when theory predicted that they could not be seen. The authors suggested that the reason for the aforementioned discrepancies might be the use of bi-Maxwellian electrons in the theory as opposed to the flat-topped electron distribution shown by the PEACE data.

The flat-top electron distribution in the magnetosheath is well known [*Feldman*, 1985]. *Chateau and Meyer-Vernet* [1989], for instance, used such a model in their calculation of the quasi-thermal noise. More recently, *Teste and Parks* [2009] reported similar flat-top distributions measured with Cluster satellite in the magnetotail, which are associated with the whistler waves triggered by the electron cyclotron resonance instability.

In this paper, we employ a non-Maxwellian distribution function that possesses a flat-top feature for low-energy electrons and a power law energetic tail distribution, namely, the (r, q) or generalized kappa distribution function, to obtain the theoretical expression for the whistler wave dispersion relation with electron temperature anisotropy, which is believed to be responsible for triggering lion roars in the magnetosheath.

The (r, q) distribution is eminently suitable for modeling the electron distributions observed in the downstream region of the terrestrial bow shock, but it can also be employed in a general situation in space plasmas. For instance, *Zaheer and Yoon* [2013] employed (r, q) distribution for modeling the solar wind electrons near 1 AU. As it will be shown, the use of (r, q) distribution significantly modifies the growth rate for electromagnetic (EM) whistler waves, such that the peculiar features in the observational data of lion roars are successfully explained, contrary to the bi-Maxwellian distribution of electrons.

2. Whistler Wave Stability Analysis With (r, q) Distribution

The generalized (r, q) distribution for the electrons is given by the form

$$f_{(r,q)} = \frac{3\Gamma(q)}{4\pi\Psi_{T\perp}^2\Psi_{T\parallel}(q-1)^{\mu}\Gamma(q-\mu)\Gamma(1+\mu)}\left[1+\frac{1}{q-1}\left(\frac{2E_{\parallel}}{aT_{\parallel}}+\frac{2E_{\perp}}{aT_{\perp}}\right)^{r+1}\right]^{-q}, \tag{1}$$

where various short-hand notations for various constants associated with the parameter r and modified parallel and perpendicular electron thermal velocities are defined, respectively, by

$$\rho = \frac{1}{1+r}, \quad \mu = \frac{3\rho}{2}, \quad \nu = \frac{5\rho}{2}, \quad a = \frac{3\Gamma(q-\mu)\Gamma(\mu)}{(q-1)^{\rho}\Gamma(\nu)\Gamma(q-\nu)}, \quad \Psi_{T\parallel} = \sqrt{a}v_{T\parallel}, \quad \Psi_{T\perp} = \sqrt{a}v_{T\perp}.$$

Here $v_{T\parallel(\perp)} = \sqrt{T_{\parallel(\perp)}/m}$ is the electron thermal velocity, $T_{\parallel(\perp)}$ is parallel (perpendicular) temperature, and m is the electron mass. The above distribution function is the generalized form of Maxwellian and kappa distribution functions. The limit of $r = 0$ and $q = \kappa + 1$ is equivalent to the kappa distribution, while the model reduces to Maxwellian distribution function when $r = 0$ and $q \to \infty$. Generally, the spectral indices r and q correspond to the flat-top (or shoulders) and high-energy tail in the profile of distribution function, respectively [*Qureshi et al.*, 2004; *Kiran et al.*, 2006].

The general dispersion relation for the right-hand (*R* wave) and left-hand (*L* wave) circularly polarized waves propagating in parallel (and antiparallel) direction with respect to the ambient magnetic field is [*Stix*, 1992; *Baumjohann and Treumann*, 1997]

$$0 = 1 - \frac{c^2k_{\parallel}^2}{\omega^2} - \frac{\omega_p^2}{2\omega}\int \mathrm{d}^3v\,\frac{v_{\perp}}{k_{\parallel}v_{\parallel} - (\omega \mp \Omega)}\left[\left(1-\frac{k_{\parallel}v_{\parallel}}{\omega}\right)\frac{\partial f_0}{\partial v_{\perp}} + \frac{k_{\parallel}v_{\perp}}{\omega}\frac{\partial f_0}{\partial v_{\parallel}}\right] = 0, \tag{2}$$

where $\omega_p = (4\pi n_0 e^2/m_e)^{1/2}$ and $\Omega = eB_0/m_e c$ are the electron plasma and cyclotron frequencies, respectively, n_0, e, B_0, m_e, and c being the customary notations indicating the ambient electron number density, unit electric charge, ambient magnetic field intensity, the electron rest mass, and the speed of light in vacuo. In equation (2), ω and $k_{\parallel}$ represent the angular frequency and (parallel) wave number, respectively. By inserting the distribution function (1) into equation (2), we obtain the general dispersion relation for *R* and *L* waves as [*Qureshi et al.*, 2004]

$$0 = 1 - \frac{c^2k_{\parallel}^2}{\omega^2} - \frac{\omega_p^2}{\omega^2}\left\{\left(\frac{\omega}{k_{\parallel}\Psi_{T\parallel}} - A_e\zeta_{\pm}\right)\left[AC_1\zeta_{\pm} + \zeta_{\pm}^2 Z_1(\zeta_{\pm}) - Z_2(\zeta_{\pm})\right] - A_e A(C_2 - BC_3)\right\},$$
$$\zeta_{\pm} = \frac{\omega \pm \Omega}{k_{\parallel}\Psi_{T\parallel}}, \qquad A_e = 1 - \frac{\Psi_{T\perp}^2}{\Psi_{T\parallel}^2} = 1 - \frac{T_{\perp e}}{T_{\parallel e}}. \tag{3}$$

In equation (3), various quantities are defined by

$$
\begin{aligned}
Z_1(\xi) &= A\int_{-\infty}^{\infty}\frac{\mathrm{d}s}{s-\xi}\left(1+\frac{s^{2+2r}}{q-1}\right)^{-q},\\
Z_2(\xi) &= AB\int_{-\infty}^{\infty}\mathrm{d}s\,\frac{s^{2-2q-2qr}}{s-\xi}F\left(1+q,q-\frac{1}{1+r};q+\frac{r}{1+r};-\frac{q-1}{s^{2+2r}}\right),\\
A &= \frac{3(q-1)^{-\mu}\Gamma(q)}{4\Gamma(q-\mu)\Gamma(1+\mu)},\\
B &= \frac{3(r+1)(q-1)^{q-\mu}\Gamma(q+1)}{4(q+qr-1)\Gamma(q-\mu)\Gamma(1+\mu)},\\
C_1 &= \int_{-\infty}^{\infty}\mathrm{d}s\left(1+\frac{s^{2+2r}}{q-1}\right)^{-q},\\
C_2 &= \int_{-\infty}^{\infty}\mathrm{d}s\,s^2\left(1+\frac{s^{2+2r}}{q-1}\right)^{-q},\\
C_3 &= \int_{-\infty}^{\infty}\mathrm{d}s\,s^{2-2q-2qr}F\left(1+q,q-\frac{1}{1+r};q+\frac{r}{1+r};-\frac{q-1}{s^{2+2r}}\right),
\end{aligned}
\tag{4}
$$

where $F(a,b;c;d)$ is the Gauss hypergeometric function.

The dispersion relation for whistler waves can be obtained by solving the expression of R wave, since no L mode is present in the cold plasma limit in the frequency range of present study. In deriving the dispersion relation, we assume that the wave frequency to be much lower than the electron cyclotron frequency and much higher than the ion cyclotron frequency, i.e., $\Omega_i \ll \omega \ll |\Omega|$, thereby ion dynamics are neglected. The real frequency and the damping/growth rate can then be written as

$$
\begin{aligned}
\omega_r &= \Omega\frac{c^2k^2}{\omega_p^2}\frac{1+A\left(BC_4-C_5\right)a\beta_{\|e}A_e}{A\left(BC_3-C_2\right)},\\
\gamma &= \frac{\pi\omega_p^2\left[\omega_r+A_e\left(\omega_r-\Omega\right)\right]}{k\Psi_{T\|}}\left[\xi^2\left(1+\frac{\xi^{2+2r}}{q-1}\right)^{-q}-B\xi^{2-2q-2qr}\right.\\
&\quad\left.\times F\left(1+q,q-\frac{1}{1+r};q+\frac{r}{1+r};-\frac{q-1}{\xi^{2+2r}}\right)\right]\\
&\quad\times\left(\frac{2c^2k^2}{\omega_r}-A\left(BC_3-C_2\right)\frac{\omega_p^2}{\Omega}+A\left(BC_4-C_5\right)\frac{\omega_p^2k^2\Psi_{T\|}^2}{\omega_r\Omega^3}\left(2A_e\Omega-\omega_r\right)\right)^{-1},
\end{aligned}
\tag{5}
$$

where the quantity a in front of $\beta_{\|e}$ in the expression for ω_r is defined in the displayed equation that appears after equation (1),

$$
\begin{aligned}
\xi^2 &= \frac{(\omega_r-\Omega)^2}{k^2\Psi_{T\|}^2}, \qquad \beta_{\|e} = \frac{2\mu_0 nk_BT_{\|e}}{B^2},\\
C_4 &= \int_{-\infty}^{\infty}\mathrm{d}s\,s^{4-2q-2qr}F\left(1+q,q-\frac{1}{1+r};q+\frac{r}{1+r};-\frac{q-1}{s^{2+2r}}\right),\\
C_5 &= \int_{-\infty}^{\infty}\mathrm{d}s\,s^4\left(1+\frac{s^{2+2r}}{q-1}\right)^{-q}.
\end{aligned}
\tag{6}
$$

It can be seen from equation (5) that the conditions for the growth rate of whistler waves with electron temperature anisotropy modeled with generalized (r,q) distribution are

$$
\frac{\omega_r}{\Omega} < \frac{A_e}{A_e+1} \tag{7}
$$

and

$$
A\left(BC_4-C_5\right) > 0. \tag{8}
$$

Both conditions (7) and (8) must be satisfied for the onset of instability. These conditions reflect the modification of the whistler instability condition under (r,q) distribution. As it will turn out, the instability condition for bi-Maxwellian distribution is necessary but not sufficient for the onset of instability. It will be shown that the modified stability conditions (7) and (8) are crucial for addressing many inexplicable features of the bi-Maxwellian theory, and as such it brings about a significant improvement to the agreement between theory and data.

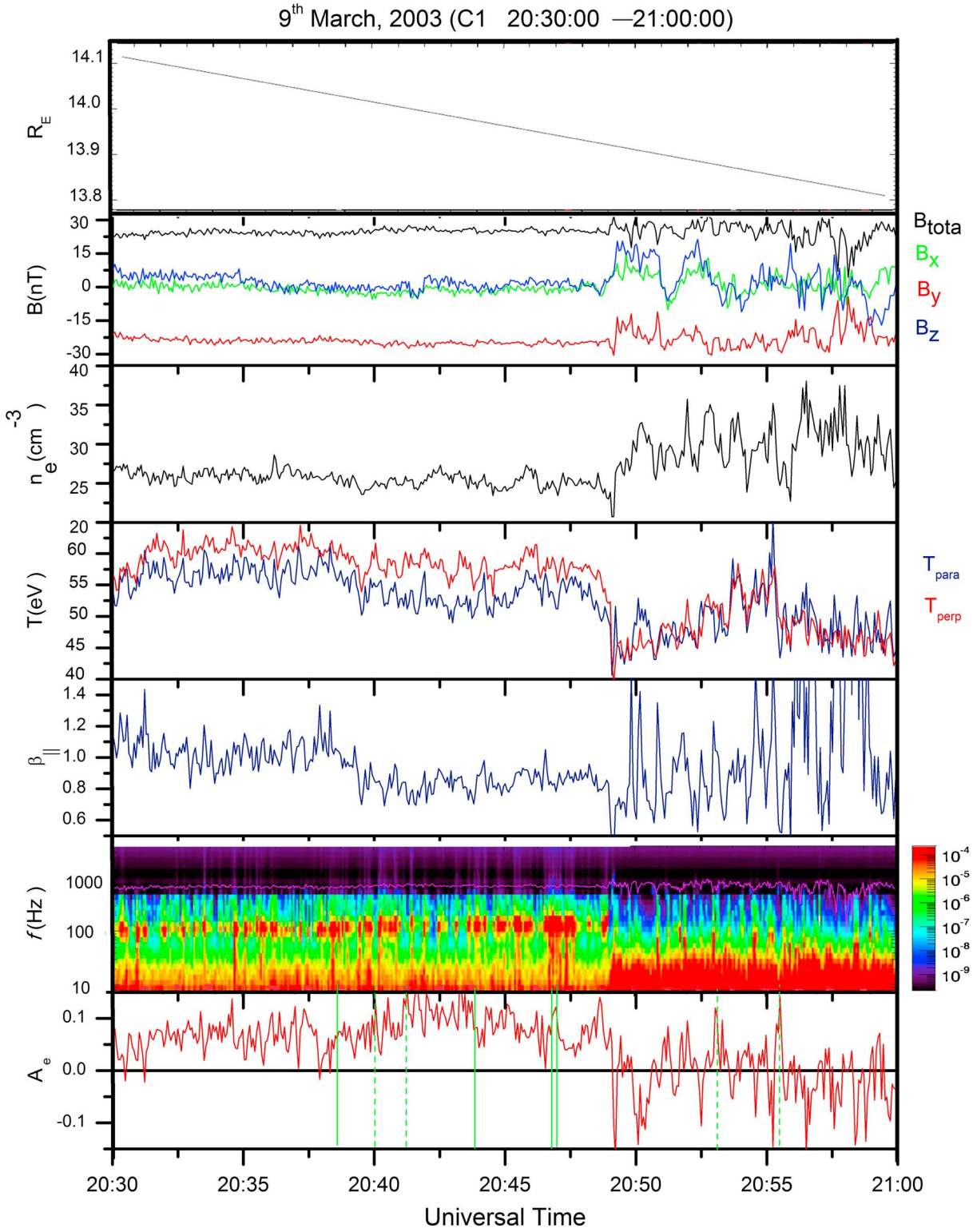

Figure 1. Cluster C1 data from 20:30:00 to 21:00:00 UT on 9 March 2003. The first panel shows the satellite position in magnetosheath in R_E, second panel shows the magnetic field components and total magnetic field. The third to fifth panels show the electron number density, parallel and perpendicular electron temperatures, and plasma beta. The sixth panel shows the frequency spectrum of the lion roars as observed from onboard STAFF data for the selected interval. The seventh panel shows the electron temperature anisotropy parameter A_e. The solid lines in the A_e panel indicate the intervals when A_e is positive and line roars are observed, and dashed lines indicate the intervals when A_e is positive and no line roars are observed in the data.

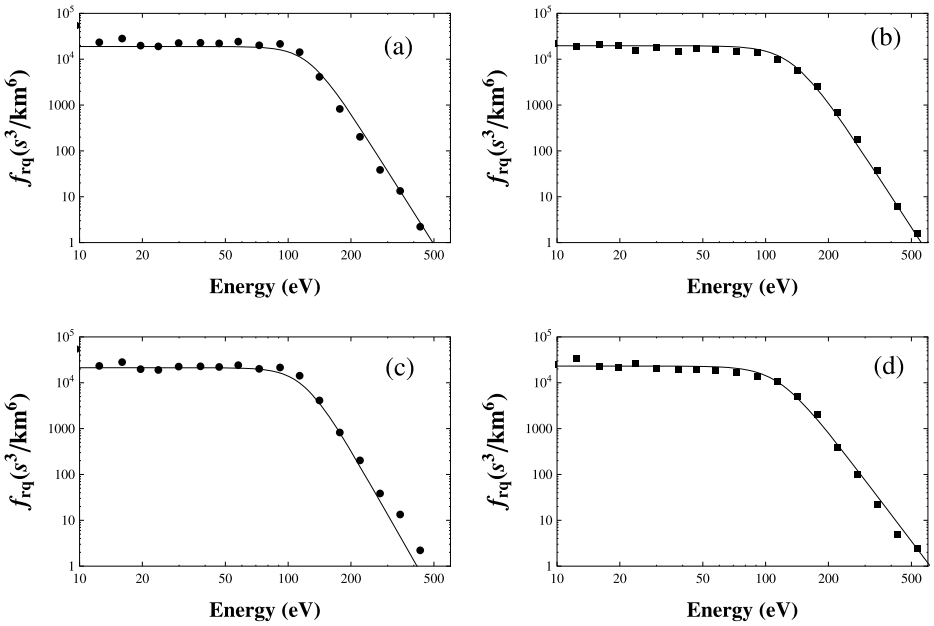

Figure 2. Parallel (solid circles) and perpendicular (solid squares) cuts of the observed distribution functions at (a and b) 20:38:31 UT and (c and d) 20:43:51 UT on 9 March 2003. Solid lines show the fits by the generalized (r, q) distribution function when (Figure 2a) $r = 5.0$ and $q = 1.2$, (Figure 2b) $r = 4.0$ and $q = 1.4$, (Figure 2c) $r = 4.8$ and $q = 1.38$, and (Figure 2d) $r = 4.0$ and $q = 1.2$ corresponding to the times when the anisotropy parameter A_e is positive and lion roars are observed in the data shown as solid lines in Figure 1.

3. Application to Magnetosheath Lion Roars

We now compare our theoretical results based on generalized (r, q) distribution with the observations of lion roars presented in the paper by *Masood et al.* [2006]. We calculate the frequency ω_r and growth rate γ for different values of spectral indices r and q that give maximum values of frequency and growth rates for the corresponding observed plasma parameters satisfying the conditions (7) and (8) simultaneously. We begin by investigating Figure 1 of the paper by *Masood et al.* [2006]. Lion roars are observed for most of the time when the temperature anisotropy parameter A_e is positive. However, there are intervals when A_e is positive, but lion roars are not observed such as 20:40:00, 20:41:11, and 20:55:00, as mentioned by *Masood et al.* [2006]. During such time intervals, the Maxwellian theory predicts the presence of lion roars in contrast to the observations. However, when we use modified damping/growth rate (5) based on the generalized (r, q) distribution, we find that condition (7) is satisfied but condition (8) is not satisfied, so that we obtain damping at those intervals instead of growth.

Figure 1 shows Cluster C1 data from 20:30:00 to 21:00:00 UT on 9 March 2003 during which lion roars are observed in the magnetosheath. Figure 1 (first panel) shows the satellite position in R_E (where R_E is the radius of Earth), Figure 1 (second panel) shows the ambient magnetic field B_{tot} along with its three components, B_x, B_y, and B_z. Figure 1 (third to fifth panels) shows the electron number density N_e, parallel and perpendicular electron temperatures ($T_{\|e}$ and $T_{\perp e}$), and plasma beta $\beta_{\|}$. The data of background magnetic field, density, parallel, and perpendicular temperatures for the selected interval have been taken from fluxgate magnetometer [*Balogh et al.*, 1997] and Plasma Electron and Current Experiment (PEACE) [*Johnstone et al.*, 1997], respectively. The sixth panel shows the frequency spectrum of the lion roars as observed from the Spatio-Temporal Analysis of Field Fluctuations (STAFF) [*Cornilleau-Wehrlin et al.*, 1997] onboard data for the selected interval. The seventh panel shows the electron temperature anisotropy parameter A_e. The solid lines in the A_e panel indicate the intervals when A_e is positive and line roars are observed in the data, whereas the dashed lines indicate the intervals when A_e is positive but no line roars are observed in the data.

Note that from 20:30 UT to ~20:47 UT, the background magnetic field and number density do not show any significant variations. The electron temperature anisotropy, A_e, however, continuously shows a variation, although it remains positive throughout. This is the time interval when lion roars are frequently observed in the data. From 20:47 UT to 21:00 UT, all the background plasma parameters show very rapid fluctuations,

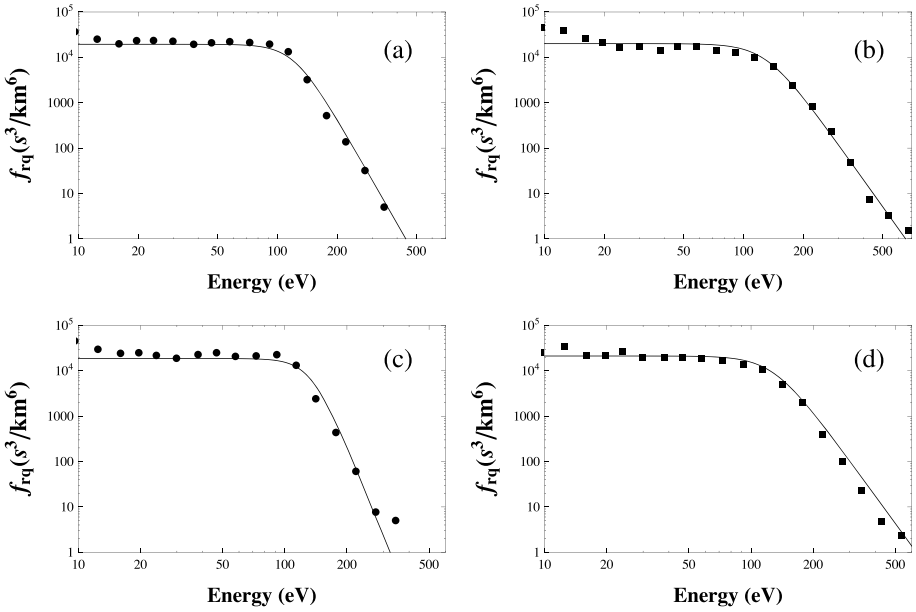

Figure 3. Parallel (solid circles) and perpendicular (solid squares) cuts of the observed distribution functions at (a and b) 20:40:00 UT and (c and d) 20:41:11 UT on 9 March 2003. Solid lines show the fits by the generalized (r, q) distribution function when (Figure 3a) $r = 4.9$ and $q = 1.3$, (Figure 3b) $r = 4.0$ and $q = 1.23$, (Figure 3c) $r = 6.0$ and $q = 1.6$, and (Figure 3d) $r = 4.0$ and $q = 1.23$ corresponding to the times when the anisotropy parameter A_e is positive but lion roars are not observed in the data shown as dashed lines in Figure 1.

and this could be due to the change of the shock geometry from quasi-perpendicular to quasi-parallel. It is pertinent to mention here that the variation of the plasma parameters downstream of a quasi-perpendicular geometry is not very pronounced. The absence of the lion roars in the STAFF data from 20:47 UT onward is due to the negative electron temperature anisotropy as well as small positive temperature anisotropy values, which might not have been enough to generate the whistler waves locally in order to be observed by the satellite. Moreover, there are instances in the data from 20:30 UT to 20:47 UT when the values of A_e are appreciably positive; however, no lion roars are observed in the STAFF data. It will be shown in later sections that employing the non-Maxwellian electron distribution, instead of the Maxwellian distribution, enables us to address these as well as other discrepancies between theory and observational data.

Figure 2 shows the fitting of the observed distribution with the generalized (r, q) distribution function when the lion roars are observed in the data and anisotropy parameter A_e is positive. In Figure 2, solid circles represent parallel cuts and solid squares represent perpendicular cuts of the observed distribution functions at 20:38:31 UT (a and b) and 20:43:51 UT (c and d), respectively, on 9 March 2003. Solid lines show the fits by the generalized (r, q) distribution function when (Figure 2a) $r = 5.0$ and $q = 1.2$, (Figure 2b) $r = 4.0$ and $q = 1.4$, (Figure 2c) $r = 4.8$ and $q = 1.38$, and (Figure 2d) $r = 4.0$ and $q = 1.2$ corresponding to the times shown as solid lines in Figure 1.

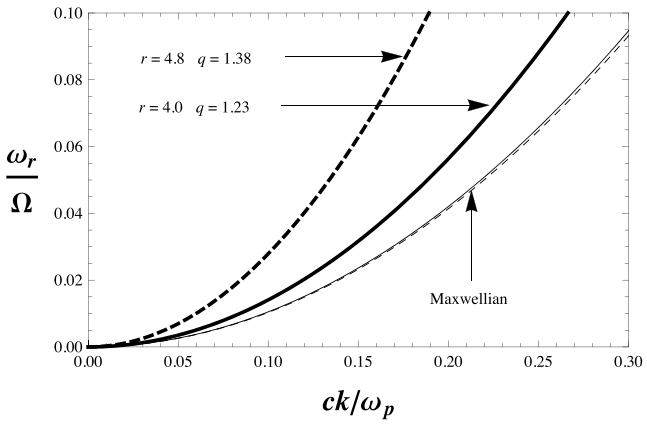

Figure 4. Real frequency for the Maxwellian case (thin lines) and generalized (r, q) distribution (bold lines) when $A_e = 0.123$ and $\beta_{\|e} = 0.842$ (solid lines) and $A_e = 0.06$ and $\beta_{\|e} = 1.05$ (dashed lines) corresponding to times 20:41:11 UT and 20:43:51 UT, respectively.

In Figure 3, solid circles represent parallel cuts and solid squares represent perpendicular cuts of the observed distribution functions at 20:40:00 UT (a and b) and 20:41:11 UT (c and d), respectively, on 9 March 2003 when lion roars are not

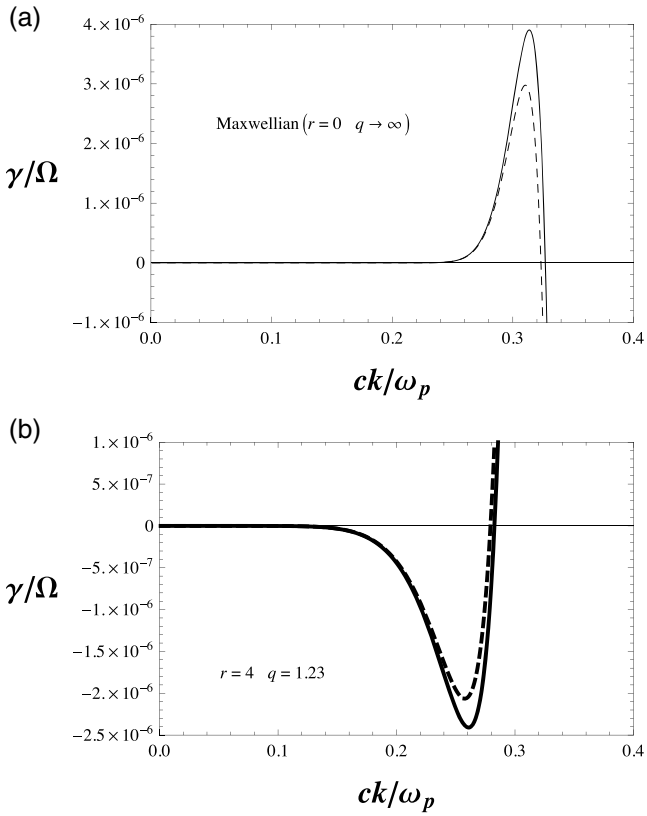

Figure 5. (a) Growth rate for the Maxwellian case and (b) damping for the generalized (r, q) distribution, when $A_e = 0.127$ and $\beta_{\|e} = 0.84$ (solid lines) and $A_e = 0.123$ and $\beta_{\|e} = 0.842$ (dashed lines) corresponding to times 20:40:00 UT and 20:41:11 UT, respectively.

observed in the data but anisotropy parameter A_e is positive shown as dashed lines in Figure 1. In Figure 3, solid lines show the fits by the generalized (r, q) distribution function when (a) $r = 4.9$ and $q = 1.3$, (b) $r = 4.0$ and $q = 1.23$, (c) $r = 6.0$ and $q = 1.6$, and (d) $r = 4.0$ and $q = 1.23$. From Figures 2 and 3, it is evident that the values of the spectral indices r and q used in the fittings clearly show the highly non-Maxwellian features especially the flat tops in the profile of distribution function. For high-energy portion, the observed distributions as well as the theoretical fits clearly show the quasi power law distribution.

For the time interval 20:41:11 UT and 20:43:51 UT on 9 March 2003, at which the fittings are shown in Figures 2 and 3, we plot real frequency in Figure 4, for $r = 4.0$ and $q = 1.23$ and $r = 4.8$ and $q = 1.38$, respectively. Figure 4 depicts the real frequency for the Maxwellian distribution (thin lines) and generalized (r, q) distribution (bold lines) when $A_e = 0.123$ and $\beta_{\|e} = 0.842$ (solid lines) and $A_e = 0.06$ and $\beta_{\|e} = 1.05$ (dashed lines). It is evident from Figure 4 that the real frequency is not sensitive to the change in parameters A_e and $\beta_{\|e}$, in the case of Maxwellian distribution. The case of generalized (r, q) distribution function shows more appreciable dependence of these parameters.

For the time interval 20:40:00 UT and 20:41:11 UT on 9 March 2003, at which the fittings are shown in Figure 3, we plot damping/growth rate in Figure 5. Figure 5a depicts the growth rate for the Maxwellian distribution function when $A_e = 0.127$ and $\beta_{\|e} = 0.84$ (solid lines) and $A_e = 0.123$ and $\beta_{\|e} = 0.842$ (dashed lines). In the case of generalized (r, q) distribution, Figure 5b depicts the case when $r = 4.0$ and $q = 1.23$ also assuming $A_e = 0.127$ and $\beta_{\|e} = 0.84$ (solid lines) and $A_e = 0.123$ and $\beta_{\|e} = 0.842$ (dashed lines). As one can see, instead of growth we obtain damping for both of the cases, which is opposite of the Maxwellian cases. So the situation can be summarized as follows: When the anisotropic parameter A_e remains positive, the Maxwellian theory predicts growth. However, when we employ generalized (r, q) distribution we obtain damping, which is consistent with the observations.

For other time intervals at which the parameter A_e remains positive and lion roars are observed in the data, both theories predict growth. However, growth remains higher for generalized (r, q) case and ranges from less than 1 s to 1.5 min, whereas the Maxwellian growth time remains as low as 17 min for 9 March 2003. This conclusion will be true throughout the following discussion unless otherwise mentioned. In order to avoid repetition, we do not show growth rate curves for these other cases. As the wave frequency is much smaller than the electron cyclotron frequency for Whistler waves, i.e., $\omega \ll |\Omega|$, an upper limit on k is obtained, so in Figure 5 we restricted the range of wave numbers to $k < 0.5$.

The damping rates depicted in Figure 5 can be translated to actual damping time measured in second, and we found the exponential damping time to be rather short (less than 1 s as shown in Table 1). Consequently, the wave damps very quickly, much before it is observed at the satellite's position. Moreover, if we consider typical downstream solar wind velocity of 100 km/s and magnetosheath thickness of 3 R_E, we expect to observe lion roars if the growth rate of the whistler waves is less than 3 min. Making use of the different

Table 1. Growth/Damping Times in Seconds Corresponding to the Anisotropy Parameter A_e, Condition (8), r and q Values for the Times When Lion Roars Are Observed and When Lion Roars Are not Observed in the Data as Indicated by Solid and Dashed Lines in Figure 1, Respectively

Time (UT)	A_e	$A(BC_4 - C_5)$	r	q	Growth/Damping Time (s)
20:38:31	0.0686	0.0234	5.0	1.20	8.56
20:43:51	0.0813	0.0526	4.8	1.38	0.62
20:46:52	0.114	0.1737	4.0	1.41	56.3
20:47:00	0.083	0.0899	4.0	1.43	1.10
20:40:00	0.127	−0.0441	4.0	1.23	−4.10
20:41:11	0.123	−0.0463	6.0	1.60	−0.80
20:53:05	0.104	−0.0441	4.0	1.23	−13.6
20:55:26	0.073	−0.1161	4.0	1.23	−22.7

values of r and q and the observed plasma parameters, we found that the growth rate from equation (5), for those data points when we see positive A_e and corresponding lion roars in the data, lies in the range of 0.5 s to 1.5 min. We also found that theoretical value of maximum frequency is about 65 Hz, whereas observed frequency is about 80 Hz [*Masood et al.*, 2006]. Therefore, we predict that lion roars are generated locally, not remotely as predicted by the Maxwellian theory [*Masood et al.*, 2006]. We note here that in the numerical estimation of the constants $C_1 - C_5$ we have taken only real values as the inclusion of the imaginary values, if any, makes only a negligible contribution.

Although Figure 2 of the paper by *Masood et al.* [2006] shows better agreement between Maxwellian theory and the observed data in that lion roars are observed for most of the time when the temperature anisotropy parameter A_e remains positive, there are also some intervals when A_e is positive but lion roars are not observed such as 20:56:28 and 21:05:00—see the paper by *Masood et al.* [2006]. For these time intervals, condition (6) is satisfied but not condition (7), so that we obtain damping instead of growth. It turns out that damping rates for these time intervals are less than or about 1 s. Other time intervals when we see positive A_e and corresponding lion roars in the data, for different values of r and q and the observed plasma parameters, growth rate lies in the range of 1 s to 1.0 min, and theoretical value of maximum frequency is about 75 Hz, which is close to the observed frequency of 80 Hz [*Masood et al.*, 2006]. Therefore, again, we predict that lion roars are generated locally and theoretical estimation of frequency has also been improved.

Figure 3 of the paper by *Masood et al.* [2006] shows the poorest agreement between Maxwellian theory and the observed data. For that interval, for most of the time, lion roars are observed but A_e remains negative. However, there are also some intervals when A_e is positive and Maxwellian theory predicts growth with a large growth time of 108 s for those intervals. However, when we consider generalized (r, q) distribution, we get growth rate times of about 20 s and frequency of about 82 Hz. Therefore, the theoretical estimates of the growth rate for this particular interval significantly improved when we use generalized distribution corresponding to the observed distribution and predict that whistler instability grows locally not in a region far from the observational site.

4. Summary

In this paper, we employed a non-Maxwellian distribution known as the generalized (r, q) distribution function in the kinetic theory of weakly damped/growing whistler waves in order to explain the observed features observed in association with the magnetosheath lion roar emission. Making use of physical input parameters taken from the observation, we find that only one condition is satisfied for the instability criteria when the bi-Maxwellian distribution is used. We found that the instability criteria based on the electron temperature anisotropy for the Maxwellian model is necessary but not sufficient, as there are numerous times when wave growth is observed in the data but theoretically damping is obtained and vice versa. Moreover, growth rates predicted by the bi-Maxwellian distribution are much lower than the growth rates deduced from the observation, suggesting that in many cases lion roars are generated far away from the observation region.

In contrast, when we employ the generalized (r, q) distribution function, the instability criteria based on the Maxwellian is modified, and we have two conditions instead of one. The growth rates theoretically obtained from generalized (r, q) distribution function substantially improve, and we propose that the lion roars are

locally generated at the site of observations, rather than being remotely generated as proposed by the Maxwellian model. In summary, we report that the model used in this paper based on the generalized (r, q) distribution function gives an excellent match with the observed values and rectifies the discrepancies that arise when the bi-Maxwellian distribution function is used. The present paper is a glittering example of the importance of non-Maxwellian space plasmas in that it resolves some long-standing uncertainties in space plasma physics.

Acknowledgments

Numerical data for generating all the figures will be made available upon request (contact information: Nouman Sarwar Qureshi [nouman_sarwar@yahoo.com]). The authors acknowledge the Cluster Active Archive (CAA) at http://caa.estec.esa.int. M.N.S. Qureshi acknowledges the Higher Education Commission (HEC), Pakistan grant 20-1886/R&D10. P.H.Y. acknowledges NSF grants AGS1138720 and AGS1242331 to the University of Maryland, and the BK21-Plus grant to Kyung Hee University, Korea, from the National Research Foundation (NRF) funded by the Ministry of Education of Korea.

Michael Liemohn thanks Eric Lund and another reviewer for their assistance in evaluating this paper.

References

Anderson, R. R., C. C. Harvey, M. M. Hoppe, B. T. Tsurutani, T. E. Eastman, and J. Etcheto (1982), Plasma waves near the magnetopause, *J. Geophys. Res.*, *87*, 2087–2107.

Balogh, A., et al. (1997), The Cluster magnetic field investigation, *Space Sci. Rev.*, *79*, 65–91.

Baumjohann, W., and R. A. Treumann (1997), *Basic Space Plasma Physics*, Imperial College Press, London, U. K.

Baumjohann, W., R. A. Treumann, E. Georgescu, G. Haerendel, K.-H. Fornacon, and U. Auster (1999), Waveform and packet structure of lion roars, *Ann. Geophys.*, *17*, 1528–1534.

Chateau, Y. F., and N. Meyer-Vernet (1989), Electrostatic noise in non-Maxwellian plasmas: "Flat-top" distribution function, *J. Geophys. Res.*, *94*, 15,407–15,414.

Cornilleau-Wehrlin, N., et al. (1997), The Cluster Spatio-Temporal Analysis of Field Fluctuations (STAFF) experiment, *Space Sci. Rev.*, *79*, 107–136.

Feldman, W. C. (1985), Electron velocity distributions near collisionless shocks, in *Collisionless Shocks in the Heliosphere: Reviews of Current Research, Geophys. Monogr. Ser.*, vol. 35, edited by B. T. Tsurutani and R. G. Stone, pp. 195–205, AGU, Washingon, D. C.

Johnstone, A. D., et al. (1997), PEACE: A plasma electron and current experiment, *Space Sci. Rev.*, *79*, 351–398.

Kiran, Z., H. A. Shah, M. N. S. Qureshi, and G. Murtaza (2006), Parallel proton heating in solar wind using generalized (r, q) distribution function, *Solar Phys.*, *236*, 167–183.

Lee, L. C., C. S. Wu, and C. P. Price (1987), On the generation of magnetosheath lion roars, *J. Geophys. Res.*, *92*, 2343–2348.

Maksimovic, M., et al. (2001), Polarization and propagation of lion roars in the dusk side magnetsheath, *Ann. Geophys.*, *19*, 1429–1438.

Masood, W., S. J. Schwartz, M. Maksimovic, and A. N. Fazakerley (2006), Electron velocity distribution and lion roars in the magnetosheath, *Ann. Geophys.*, *24*, 1725–1735.

Moreira, A. (1983), Stability analysis of magnetosheath lion roars, *Planet. Space Sci.*, *10*, 1165–1170.

Qureshi, M. N. S., H. A. Shah, G. Murtaza, S. J. Schwartz, and F. Mahmood (2004), Parallel propagating electromagnetic modes with the generalized (r, q) distribution function, *Phys. Plasmas*, *11*, 3819, doi:10.1063/1.1688329.

Rodriguez, P. (1985), Long duration lion roars associated with quasi-perpendicular bow shocks, *J. Geophys. Res.*, *90*, 241–248.

Smith, E. J. (1969), Magnetic emissions in the magnetosheath at frequencies near 100 Hz, *J. Geophys. Res.*, *74*, 3027–3036.

Smith, E. J., and B. T. Tsurutani (1976), Magnetosheath lion roars, *J. Geophys. Res.*, *81*, 2261–2266.

Stix, T. H. (1992), *Waves in Plasmas*, 247 pp., AIP, New York.

Teste, A., and G. K. Parks (2009), Counterstreaming beams and flat-top electron distributions observed with Langmuir, whistler, and compressional Alfvén waves in Earth's magnetic tail, *Phys. Rev. Lett.*, *102*, 75003.

Thorne, R. M., and B. T. Tsurutani (1981), Generation mechanism for magnetosheath lion roars, *Nature*, *293*, 384–386.

Tsurutani, B. T., E. J. Smith, R. R. Anderson, K. W. Ogilvie, J. D. Scudder, D. N. Baker, and S. J. Bame (1982), Lion roars and nonoscillatory drift mirror waves in the magnetosheath, *J. Geophys. Res.*, *87*, 6060–6072.

Zaheer, S., and P. H. Yoon (2013), On quiet-time solar wind electron distributions in dynamical equilibrium with Langmuir turbulence, *Astrophys. J.*, *775*, 108, doi:10.1088/0004-637X/775/2/108.

Zhang, Y., H. Matsumoto, and H. Kojima (1998), Lion roars in the magnetosheath: The Geotail observations, *J. Geophys. Res.*, *103*, 4615–4626.